JACS
JOURNAL OF THE AMERICAN CHEMICAL SOCIETY
Article
pubs.acs.org/JACS

Low-Molecular-Weight Carbon Nitrides for Solar Hydrogen Evolution

Vincent Wing-hei Lau,[†,§] Maria B. Mesch,[‡] Viola Duppel,[†,§] Volker Blum,[∥] Jürgen Senker,[‡] and Bettina V. Lotsch*[,†,§,⊥]

[†]Max Planck Institute for Solid State Research, Heisenbergstraße 1, 70569 Stuttgart, Germany
[‡]Department of Inorganic Chemistry III, University of Bayreuth, Universitätsstraße 30, 95447 Bayreuth, Germany
[§]Department of Chemistry, University of Munich, Butenandtstraße 5-13, 81377 Munich, Germany
[∥]Department of Mechanical Engineering and Materials Science and Center for Materials Genomics, Duke University, Durham, North Carolina 27708, United States
[⊥]Nanosystems Initiative Munich (NIM) and Center for Nanoscience, Schellingstraße 4, 80799 Munich, Germany

Supporting Information

ABSTRACT: This work focuses on the control of the polymerization process for melon ("graphitic carbon nitride"), with the aim of improving its photocatalytic activity intrinsically. We demonstrate here that reduction of the synthesis temperature leads to a mixture of the monomer melem and its higher condensates. We show that this mixture can be separated and provide evidence that the higher condensates are isolated oligomers of melem. On evaluating their photocatalytic activity for hydrogen evolution, the oligomers were found to be the most active species, having up to twice the activity of the monomer/oligomer mixture of the as-synthesized material, which in turn has 3 times the activity of the polymer melon, the literature benchmark. These results highlight the role of "defects", i.e., chain terminations, in increasing the catalytic activity of carbon nitrides and at the same time point to the ample potential of intrinsically improving the photocatalytic activity of "carbon nitride", especially through the selective synthesis of the active phase.

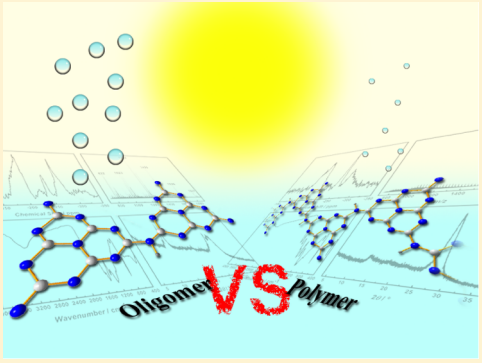

INTRODUCTION

Hydrogen production by photocatalytic water splitting is a promising technology for the storage and direct conversion of solar into chemical energy. The chemical energy can then be extracted using, for example, fuel cells with high efficiency, yielding only water as the byproduct. This cycle forms the basis of the energy paradigm known as the "hydrogen economy", a sustainable and environmentally benign alternative to the current practice based on the combustion of fossil fuels.[1] Following the seminal publication of Honda and Fujishima on TiO_2-photocatalyzed water splitting four decades ago,[2] many photocatalytic materials have been identified, of which the most active ones include La-doped $NaTaO_3$[3] and the solid solution $Ga_{0.88}Zn_{0.12}N_{0.88}O_{0.12}$.[4] However, none of these photocatalysts satisfies the requirements for commercial application, as they often require complex synthetic processes or are composed of rare and expensive elements, making their preparation uneconomical. Furthermore, many of these materials, especially the oxides, have low photocatalytic activity under visible light, the main constituent of solar irradiation at sea level.[5]

One new and promising class of photocatalysts is the so-called "graphitic carbon nitride", which are polymers based on the condensation products of melem (2,5,8-triamino-tri-striazine, Scheme S1, Supporting Information).[6−8] Note that the term "graphitic carbon nitride" or "g-C_3N_4" is used only to keep consistency with the literature; it is in fact a misnomer considering that these materials do not possess the stoichiometric ratio C_3N_4 but always contain a sizable amount of hydrogen (≈2 wt %), consistent with the composition of Liebig's melon, $C_6N_9H_3$, a 1D carbon nitride polymer. Originally inspired by the "harder than diamond" postulate,[9] this family of materials were thought to be a precursor to the predicted β-C_3N_4 and have been heavily investigated for their synthetic pathway and structure.[10−16] The main advantages of these materials as photocatalysts are that they can be facilely synthesized by heat treatment of inexpensive precursors (e.g., melamine or dicyandiamide), are active under visible light irradiation, and are chemically stable. Although their photocatalytic activity is low compared to the record holders mentioned above, there are still significant avenues for performance enhancement. Some strategies for improving their activity include texturization or morphology control to increase the surface area,[17−22] chemical modification to red-shift the absorption edge,[23−26] and band alignment by coupling with other semiconductors, photocatalysts, and cocatalysts to improve the electron−hole separation.[27−34]

Received: April 9, 2014
Published: December 24, 2014

DOI: 10.1021/ja511802c
J. Am. Chem. Soc. 2015, 137, 1064−1072

Despite the growing number of publications exploring these strategies, the literature has focused almost entirely on the polymer melon as the photocatalyst and overlooked the rich diversity of other related carbon nitride materials with different degrees of polymerization. For example, a change in synthesis conditions (temperature, pressure, atmosphere, or synthesis medium) can yield a variety of phases, including oligomers and polymers of triazine, adduct phases of melem, coordination and hydrogen-bonded compounds.[15,35−38] Recent results have shown that not only are triazine polymers active for photocatalytic hydrogen and oxygen evolution, but also chemical modifications can enhance their activity to values even exceeding that of the heptazine polymer, melon.[39,40]

Another sparsely explored topic concerns the fundamental properties of these carbon nitride materials, particularly the nature of the active species, its mechanistic operation, and strategies to intrinsically improve their activity, rather than extrinsically by red-shifting the absorption through doping and increasing the surface area through morphology control. Since highly crystalline melem and melon, obtainable only by synthesis in closed ampules under an autogenous pressure of ammonia (which induces partial de- and repolymerization, thereby leading to defect healing[14]), have negligible photocatalytic activity, the currently accepted postulate is that "surface terminations and defects seem to be the real active sites".[7] A more detailed understanding of its catalytic aspects can provide the guiding principles for bottom-up design and synthesis of carbon nitride photocatalysts, particularly when many synthetic modifications are now available for the heptazine skeleton.[41]

Thus, to gain further insights into the nature of the active sites and identify the criteria necessary for photocatalytic activity in the carbon nitride family, we direct our focus away from the polymer. Specifically, we investigate here the synthesis and characterization of a carbon nitride material with lower molecular weight than the polymer, and how its structural features affect its performance for photocatalytic hydrogen evolution when compared to the polymer.

RESULTS AND DISCUSSION

In our methodology, we selected synthetic conditions that favor the condensation of melamine into melem and higher condensation products but not completely to melon (temperatures between 380 and 490 °C based on results from temperature-programmed XRD and thermogravimetric analysis).[15,42] We also employed an open vessel rather than a closed ampule, such that the ammonolytic depolymerization did not occur, thus favoring the kinetically rather than thermodynamically driven formation of low condensed melem oligomers, in line with the increased formation of chain terminations.

The product obtained at the reduced synthesis temperature of 450 °C for 12 h of calcination at 5 °C min^{-1} heating ramp, tentatively notated as "as-synthesized melem oligomer", exhibited a photocatalytic activity more than twice that of melon in acidic, neutral, or alkaline conditions under AM 1.5 conditions (Figure 1 and Figure S2, Supporting Information). Here, the benchmark material melon was synthesized at 550 °C for 12 h in argon, corresponding to the typical literature protocols;[43] crystalline melon was not used, as we have verified its negligible activity. The photocatalytic activity of the as-synthesized melem oligomer was sustained for over 120 h without any decrease, demonstrating that the catalyst stability is comparable to melon. As will be shown and discussed in more detail below, the as-synthesized melem oligomer absorbs less in the visible spectrum than melon, indicating that its better activity is not due to collection of more photons but rather either due to improved charge separation or to interfacial charge transfer.[44,45] We consider improved charge separation as an unlikely (albeit not ruled out) explanation for the better activity, since the photoexcited charge carriers in carbon nitrides have a short lifetime and appear to be confined to the individual heptazine unit without diffusing along the polymer or oligomer.[46,47] The latter explanation appears more likely, and suggests that the melem oligomer contains features that accelerate the oxidation of methanol or reduction of hydrogen via the platinum centers. These encouraging photocatalysis results thus motivated us to determine the identity of this melem oligomer, with the aim of elucidating the properties or criteria for superior photocatalytic activity in carbon nitride materials.

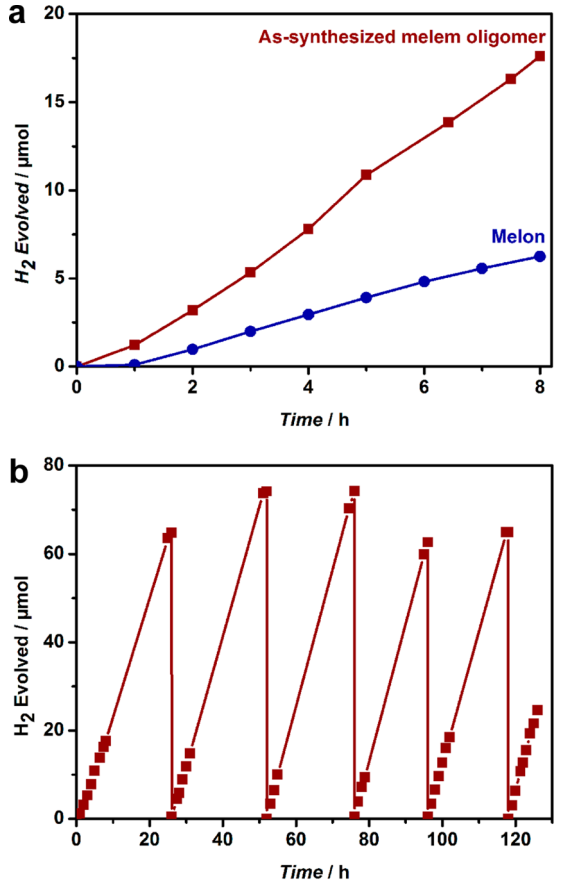

Figure 1. (a) Photocatalytic hydrogen evolution of the as-synthesized melem oligomer, compared with melon. (b) Extended photocatalytic test for 129 h of the as-synthesized melem oligomer, both in a pH 7 phosphate buffer system (PBS). After every overnight run, the reactor headspace was evacuated and purged with argon. Methanol (500 μL) was added on the 52nd and 118th hour after the overnight run.

The XRD pattern of the as-synthesized melem oligomer, depicted in Figure 2a, is similar to melem but shows various small shifts in the reflection positions, indicating that the crystalline portion of the oligomer sample contains a melem-related structure that has been observed and employed for synthesizing melem derivatives in the literature.[48] TEM analysis of the heat-treated melem oligomer (Figure S4, Supporting Information) showed the sample to have a sheet-like morphology, with lateral dimensions in the micron scale.

DOI: 10.1021/ja511802c
J. Am. Chem. Soc. 2015, 137, 1064−1072

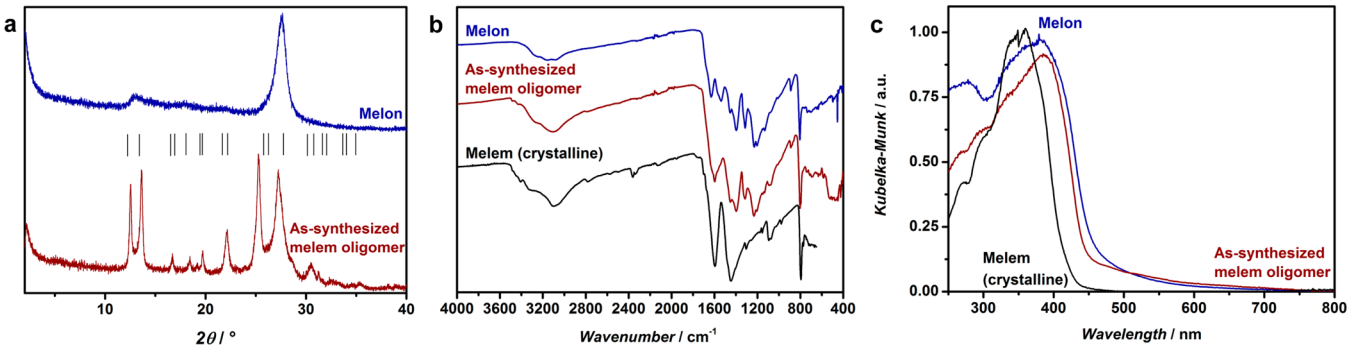

Figure 2. (a) XRD patterns, (b) ATR-IR, and (c) diffuse reflectance UV−vis spectra of the melem oligomer and melon in comparison with that of crystalline melem. The tick marks in the XRD show the prominent peaks of melem from the literature.

Electron diffraction analysis of this as-synthesized melem oligomer sample shows the presence of melem, an example given in the center image of Figure S4 (Supporting Information). An additional, melem-related phase was also observed by electron diffraction (Figure S4, Supporting Information, right) with slightly increased *d*-spacing for both 002 and 011, consistent with the melem-related phase in the XRD mentioned above. While carbon nitrides have been synthesized under similar conditions before, e.g., Guo et al. performed the synthesis under identical conditions except in air,[49,50] we found that synthesis in air worsened the reproducibility of the XRD pattern and also reduced the photocatalytic activity (which may hint at the negative effect of oxygenated or oxidized functionalities).

Despite the fact that only the monomer is observed by crystallographic techniques in the as-synthesized melem oligomer sample, results from ATR-IR and diffuse reflectance UV−vis spectroscopy (Figure 2b and c), as well as elemental analyses (Table S1, Supporting Information), are consistent with those expected of higher condensation products of melem. In the IR spectra, the absorption bands at 1206 and 1235 cm^{-1} and 1316 cm^{-1} have been shown to be characteristic of the C−NH−C unit in melam (triazine−triazine dimer, Scheme S1, Supporting Information), and thus assigned to bridging secondary amine units.[51] We also note that the UV−vis absorption for melem oligomer is between that of melem and melon. Assuming that melon behaves like a partially π-conjugated heptazine polymer,[6] this result suggests that the aromatic system is larger than the monomer but smaller than the polymer. We however caution that recent optical investigations question this organic semiconductor model, with results from photoluminescence decay showing instead that the electronic structure of g-C_3N_4 can rather be described as that of a "quasi-monomer", that is, a low degree of delocalization between the individual heptazine units.[47,52] A separate explanation independent of the semiconductor model is that the melem oligomer contains an amount of reacted primary amines between that of the monomer and polymer, since derivatization of the amines on melem can also red-shift its absorption.[48]

Lastly, the C:N atomic ratio of the as-synthesized melem oligomer sample lies between that of melem and the theoretical C_3N_4, indicating an increased degree of condensation compared to melem. Combined with the XRD and TEM analyses, these results suggest that this melem oligomer sample contained a mixture of crystalline heptazine monomers (i.e., melem) and more highly condensed but less crystalline products. While we do not rule out the possibility of forming triazine oligomers or oligomers between melem and melamine, we believe their presence to be improbable on thermodynamic considerations. For example, melam is a short-lived intermediate in the synthesis of melem,[15] while polymers of triazine are not expected to form unless under ionothermal conditions.[39]

Characterization of the spent as-synthesized catalyst after the photocatalytic reaction showed the formation of a melem hydrate phase,[38] as evident in the XRD patterns, but virtually no change in the IR spectra, from both the 8 h and the extended 129 h experiments (Figures S5 and S6, Supporting Information, respectively). The hydrate phase is likely formed from the recrystallization of the monomers present in the sample under the aqueous conditions of the photocatalytic reaction, rather than depolymerization of the higher condensation species, since the IR absorption bands corresponding to the bridging secondary amines are still present.

HRTEM analyses of the spent catalyst (Figure S7, Supporting Information) showed the formation of spherical platinum particles of diameter 1−2 nm on the catalyst surface as found previously.[43] X-ray photoelectron spectroscopy (XPS) of the spent catalyst shows the Pt $4f_{7/2}$ peak (Figure S8, Supporting Information, top right) to have a binding energy (B.E.) of around 71.3 eV, which is assigned to Pt^0. This thus confirms the formation of metallic platinum, although HRTEM and XPS naturally do not allow us to determine the molecular binding sites of the metal particles to the light harvester. The integrity of the melem oligomer was also corroborated from spectra in the C 1s (Figure S8, Supporting Information, bottom left) and N 1s regions (Figure S8, Supporting Information, bottom right). The C 1s peak at 288.1 eV has been assigned to a C−N−C coordination, while the N 1s peaks at 398.6, 399.4, and 401.2 eV have been assigned to the C−N−C group, the tertiary nitrogen $N-(C)_3$ group, and the hydrogen-bearing amine group, respectively.[53] The larger intensity of the peak at 401.2 eV, compared to literature spectra, can be attributed to the presence of the monomer melem in the sample, which is in line with our observations outlined above.[54] No change is discernible when comparing the C 1s and N 1s spectra of this material before and after the photocatalytic reaction, other than the absence of platinum.

As we are interested in elucidating the structure−property−activity relationship in carbon nitride photocatalysts, it is thus necessary to separate these higher condensation species in the sample from the monomer, which has not been reported to possess photocatalytic activity. Since DMSO can solubilize

DOI: 10.1021/ja511802c
J. Am. Chem. Soc. 2015, 137, 1064−1072

melem[13] but does not affect the polymer chemically, we therefore can remove the majority of the monomer from the bulk melem oligomer sample and isolate the oligomer, which will have a lower solubility in DMSO. The insoluble component was further separated by differential centrifugation at RCF (relative centrifugal force) values of 10000 and 60000. Descriptions of the fractions are summarized in Table 1, and

Table 1. Fractions Obtained by Differential Centrifugation of a DMSO Suspension Containing Melem Oligomer (400 mg in 100 mL)

	amount recovered (mg)	appearance
DMSO soluble	175 (48%)	white
fraction RCF 60000	57 (16%)	off-white/light yellow
fraction RCF 10000	132 (35%)	light yellow

their characterizations by XRD, UV–vis, IR, MALDI-TOF-MS, and solid-state ^{13}C and ^{15}N magic angle spinning (MAS) NMR spectroscopy are shown in Figure 3. MALDI-TOF spectra of the fractions at lower mass ranges are shown in Figure S9 (Supporting Information). A summary of the BET surface areas, photocatalytic hydrogen evolution rate, and quantum efficiencies are given in Table S2 (Supporting Information).

In the DMSO soluble fraction, the most intense reflections in the XRD coincide with the 011 and 212 reflections of melem hydrate, the water likely originating from residual moisture in the DMSO. Thus, this fraction can be assigned to the hydrate phase, indicating that melem from the as-synthesized sample was reorganized into the hydrate phase during the separation procedure, while keeping the molecular structure and integrity of the triamino-heptazine. A small amount of sulfur (~1 wt %) was detected only in this fraction (but not the other two) by elemental analysis using energy dispersive X-ray spectroscopy (EDX), which we attribute to the minute presence of a DMSO-solvate of melem.[55] Its IR spectrum shows two broad bands at 1596 and 1442 cm^{-1}, again coinciding with those of melem, while the lack of absorption at around 1231 cm^{-1} indicates the absence of the oligomeric species in this fraction. Its absorption onset in the UV–vis spectra, which is below 400 nm, suggests an underivatized monomeric structure. The ^{13}C NMR spectrum exhibits two signal groups at 164 ppm and at 155 ppm which can be assigned to the amine-bearing and the remaining heptazine carbons, respectively. In crystalline melem, both signals exhibit a fine structure, due to different hydrogen bonding environments.[10] Owing to the weak crystallinity, the signals for the present material are not as resolved and slightly shifted to lower ppm values similar to melem hydrate.[38] Three

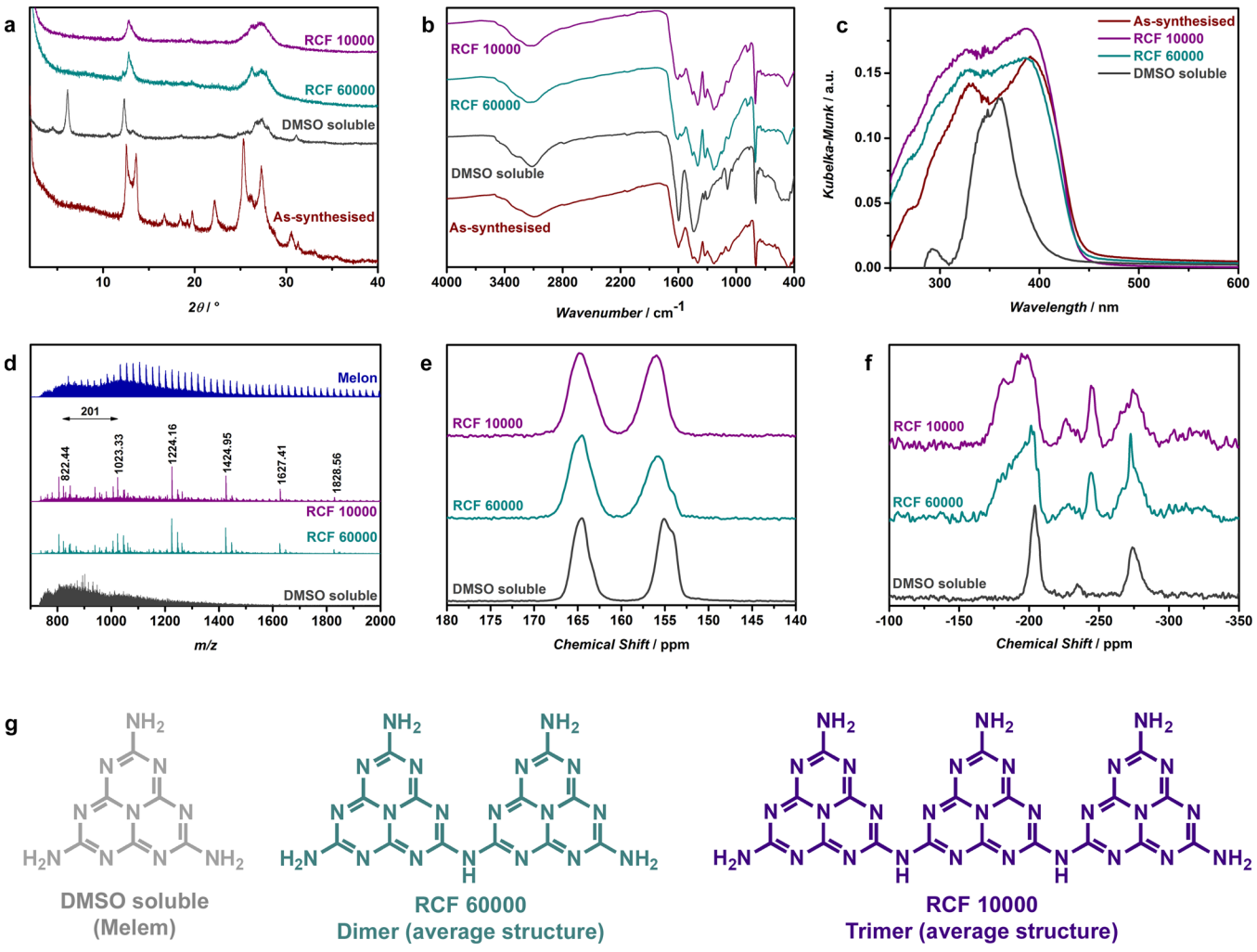

Figure 3. (a) XRD patterns, (b) ATR-IR, (c) diffuse reflectance UV–vis, (d) MALDI-TOF at mass range >850 amu in positive mode, (e) ^{13}C and (f) ^{15}N solid state CP-MAS NMR spectra, and (g) the postulated average structures of the three fractions from differential centrifugation.

DOI: 10.1021/ja511802c
J. Am. Chem. Soc. 2015, 137, 1064–1072

peaks in the ^{15}N can thus be assigned: the broad signal in the range of −190 to −210 ppm corresponds to the peripheral nitrogens in the heptazine ring, −229 to −240 ppm to the center nitrogen of heptazine, and −265 to −285 ppm to the amine. The values of these shifts coincide with those of melem or melem hydrate.[10,38] Lastly, the mass spectroscopy showed peaks at 219 and 420 amu (Figure S9, Supporting Information), corresponding to the protonated forms of the monomer and the dimer, respectively, but nothing of higher mass. It is possible that the dimer is somewhat soluble in DMSO, or may be present as a contaminant in minute amount below the detection limit of NMR (≈5%). From this characterization, we can conclude that the DMSO-soluble fraction is predominantly melem, illustrating the separation of the monomer from the higher condensates.

The other two fractions showed similarities in their IR spectra with that of melon, the noteworthy feature being the bridging amine absorption at 1231 cm^{-1}, while their UV−vis absorption onsets are in the visible region. Compared with melon, their XRD patterns exhibit a relatively sharp reflection at 12.8° 2θ and broad reflections in the range 25−29° 2θ, suggesting long-range order to some extent across the plane and largely turbostratic disorder in the stacking direction. These two fractions are however differentiated by their NMR spectra. In the ^{13}C spectrum, the RCF 60000 fraction is characterized by the same shoulder at 154 ppm as the DMSO soluble fraction, suggesting a more melem-like carbon environment. Nonetheless, both of these fractions are unequivocally not the monomer, as evidenced by the peak at −245 ppm in the ^{15}N spectrum, which coincides with the secondary amine (NH group) in melon. We also note the expansion of the signal of the peripheral heptazine nitrogens toward higher ppm values, being characteristic for melon;[14] this peak is more intense for the RCF 10000 than the 60000 fraction. Lastly, we emphasize that the shift of the central heptazine nitrogen provides information regarding the extent of the polymerization, since this peak shifts from −234 ppm for melem to −225 ppm for the polymer.[10,14] Although this peak is broad for both fractions, a comparison of the maxima revealed that the shift is at −226 ppm for the RCF 10000 fraction, whereas it is at −228 ppm for the RCF 60000 fraction, thus suggesting that this latter fraction is less melon-like than the former. An additional qualitative (but by no means quantitative, due to cross-polarization conditions) measure of polymerization is to compare the integral ratios of the $^{15}NH_2$:^{15}NH peaks in the different spectra. In this case, this ratio is around 3.3 and 2.4 for the RCF 60000 and 10000 fractions, respectively, indicating that the former has more unreacted primary amine groups, i.e., less degree of polymerization. As the ratio depends on the chain length (Figure S10, Supporting Information), the size of the oligomer can thus be approximated. Therefore, the less dense fraction (RCF 60000) with a ratio of 3.3 will mainly consist of dimers with an average length of 2.3 melem units and only a small amount of higher condensates, whereas the denser fraction (RCF 10000) is shifted toward higher condensates, mostly trimers with an average length of 3.2 melem units. The postulated structures of these two fractions as linear polymers are shown in Figure 3g. Note that, as these fractions are inevitably mixtures, the oligomer lengths shown are average structures that are consistent with the NMR results. While we do not rule out the possibility of nonlinear structures (e.g., dendrimer or cyclic structures[35]), no signal corresponding to a tertiary amine was detected from the ^{15}N NMR spectrum. We therefore surmise that nonlinear structures involving a tertiary nitrogen are either absent or present only in negligible amounts. Regarding the possible presence of triazine moieties, we note that the spectral signatures of the ^{13}C and ^{15}N 1D spectra clearly fit better to a heptazine-based oligomer, rather than a triazine-based one.

As spectral overlap could mask the minute presence of such triazine species, we have performed matrix-assisted laser desorption/ionization time-of-flight (MALDI-TOF) mass spectrometry to corroborate the NMR results. Both samples exhibit peaks at mass corresponding to the protonated monomer (219 amu), dimer (420 amu) and trimer (621 amu); further increments of 201 amu corresponding to every additional monomer up to the nonamer (1627 amu) can be also clearly resolved. No triazine-containing oligomer was observed. These signals are unlikely to be fragments of the polymer, since the spectrum for melon does not contain these peaks. In contrast, in analyzing melon in the high mass range, a series of peaks with mass separated by 24 amu was observed. Note that this separation is also observed for the RCF 10000 fraction, and is assigned to the C_2 fragment resulting from the high laser power required to generate sufficient signal intensity. While we acknowledge previous MALDI-TOF analysis of heptazine polymers showing mass intervals of 201 amu,[56] we emphasize that the spectra in this work cleanly show the molecular peaks at the exact masses expected for the oligomer, rather than the fragments. Although MALDI-TOF was unable to differentiate between these two fractions in terms of their oligomer length, it nonetheless verifies our hypothesis that these are indeed isolated oligomers of melem.

The thermal properties of these fractions and evolved volatiles were analyzed by thermogravimetric analysis coupled with mass spectroscopy under an argon atmosphere (Figure S11, Supporting Information). Melon has one mass loss step, beginning at around 520 °C accompanied by evolution of HCN, before complete decomposition takes place at 620−700 °C with the evolution of C_2N_2 and small amounts of NH_3. The DMSO soluble fraction—identified above to be melem—undergoes two mass loss steps, the first beginning at around 350 °C with evolution of ammonia and small amounts of HCN, which we attribute to the condensation polymerization of the monomer. The second step is similar to melon decomposition, with HCN and C_2N_2 evolution onset at around 520 and 600 °C, respectively. Both RCF 10000 and 60000 fractions have an identical mass loss profile with a single step mass loss at a temperature between that of the monomer and the polymer, consistent with the fact that these fractions are intermediates between the monomer and the polymer. The condensation reaction, as in melem, was not detected, and can be rationalized by the negligible presence of the monomer as a precursor.

The RCF 60000 fraction has a layered structure similar to the plate-like morphology observed in crystalline particles of melon,[14,20] as shown in its SEM (Figure S12, Supporting Information) and TEM (Figure 4), with lateral dimensions in the micron regime. These fractions were tested for photocatalytic hydrogen evolution at pH 7 under irradiation from visible light (>420 nm), and the results are shown in Figure 5. The DMSO-soluble fraction, which we have assigned to melem, exhibited negligible activity as expected, since its absorption onset is in the UV region. The fractions collected at RCF 10000 and 60000, which together constitute about 50% of the total weight of the original sample, exhibited a hydrogen evolution rate of 4.8 and 5.4 μmol h^{-1}, respectively, with an apparent quantum efficiency (AQE) estimate at 400 ± 25 nm of 0.087

DOI: 10.1021/ja511802c
J. Am. Chem. Soc. 2015, 137, 1064−1072

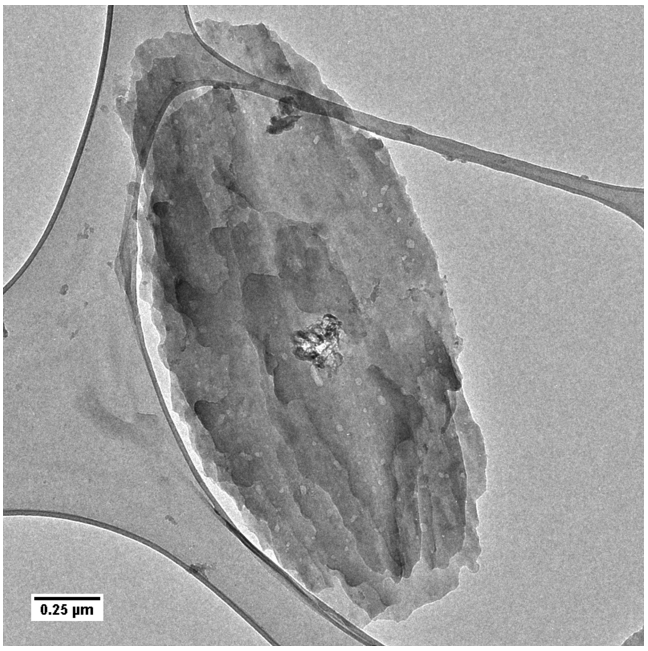

Figure 4. TEM image of the fraction obtained at RCF 60000.

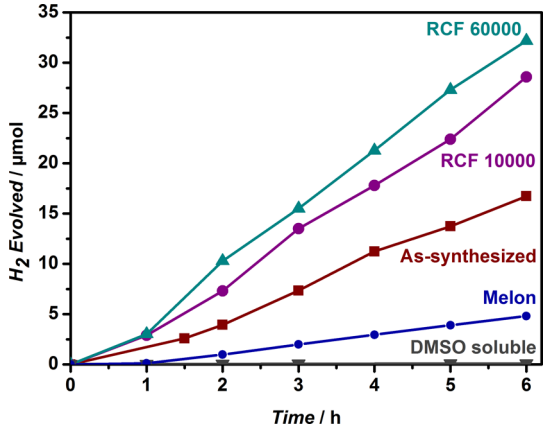

Figure 5. Photocatalytic activity under visible light irradiation ($\lambda > 420$ nm) of the fractions in PBS (18 mL of 0.1 M solution at pH 7) containing methanol (2 mL) and dihydrogen hexachloroplatinate (5 μL of 8 wt % aqueous solution). The catalyst loading in all cases was 20 mg.

and 0.1%; these hydrogen evolution rates outperformed the as-synthesized sample by 1.66 and 1.71 times, respectively, and outperformed the polymer (0.9 μmol h^{-1}, AQE 0.015% at 400 ± 25 nm) by 5.9 and 6.1 times, respectively. The BET surface areas of these two active fractions are no more than 3 times that of the polymer (see Table S2, Supporting Information), nor does their morphology differ significantly from melon (other than having a small particle size in general as a result of the differential centrifugation). Solvent interaction and dispersibility of the polymer and the RCF 10000 fraction are also quite similar, as gauged by zeta potential measurements (Figure S13, Supporting Information), which show that the polymer and this fraction has zeta potentials of −18 and −28 mV at pH 6.6 and isoelectric points of pH 3.3 and pH 2.7, respectively. The values for the polymer are in broad agreement with literature values.[27] Thus, while textural properties, solvent effects, and mass transport may have an effect on the photocatalytic performances, the vast activity differences of the fractions indicate that these attributes are not the dominating contributors but point toward other intrinsic factors as the principal explanation for the large outperformances of the oligomeric fractions, i.e., increased activity per surface area. The separation procedure using DMSO does not affect the heptazine polymer chemically, thereby ruling this factor out as the source of the increased intrinsic activity. We then consider the common explanations for intrinsic increase in activity in photocatalysis, which are (1) improvement in light absorption, (2) lengthened lifetime of photogenerated charges, and/or (3) interfacial charge transfer rate. We can rule out the first factor immediately, as these active fractions absorb less in the visible region than the polymer, based on their diffuse reflectance UV−vis spectra. These active fractions are also poorly crystalline from the XRD, a factor usually associated with enhanced electron−hole recombination and impeded charge percolation.[57] Furthermore, the carrier lifetime and mobility of heptazine polymers are considered to be unfavorable for photocatalysis, due to strong carrier localization.[47,58−60] The lifetime/mobility interplay may be varied slightly by changing the stacking separation, with the distance directly correlated with carrier lifetime but inversely correlated to mobility.[47] This relation however may not be applicable for oligomers due to differences in crystal structure and cofacial distances in the aromatic units.[47] We thus consider the second factor—increased activity due to more favorable carrier dynamics—an improbable explanation for the large difference in activity (even after normalizing the oligomers' activities to surface area; see below). Therefore, the remaining explanation, that the high activity of the as-synthesized melem oligomer is attributable to faster extraction of the photogenerated charges (i.e., faster kinetics for interfacial charge transfer), is considered the likeliest explanation. This step is typically the slowest and thus the bottleneck in most photocatalytic systems. Faster transfer kinetics can result from the catalyst having a larger number of exposed reactive sites, which may be a surface area effect. However, when the activities are normalized to the BET surface area, we see that the activity of the RCF 60000 fraction at 11 μmol h^{-1} m^{-2} has more than twice the activity of the polymer (5.3 μmol h^{-1} m^{-2}), thus illustrating that the surface area cannot be the principal factor in explaining this outperformance.

To understand the high activity of the oligomers, we have undertaken calculations of the HOMO/LUMO orbitals of the mono- and oligomers and their variation with conformation, employing van der Waals-corrected density functional theory[61,62] for the structure and an optimized hybrid functional[63] to validate orbital energy trends, using the FHI-aims all-electron code[64,65] (orbitals represented in Figure 6 and Table S4, Supporting Information; energies summarized in Table S3, Supporting Information; conformational variations in Table S4, Supporting Information; and additional discussions in the Supporting Information). The computational trends are corroborated with photoluminescence (PL) experiments (Figure S14, Supporting Information). Consistent with a previous study on the correlation of band gap with degree of polymerization,[52] the energy gap was found to expand with shorter oligomer length. Current Kohn−Sham density functional approximations cannot be expected to give absolute band gap energies, but the trend of the band gap and HOMO/LUMO energies is consistent across different functionals. For the optimized functional (PBE[61] functional), the gas-phase electronic gap increases from 7.83 (2.68) eV for the tetramer to

DOI: 10.1021/ja511802c
J. Am. Chem. Soc. 2015, 137, 1064−1072

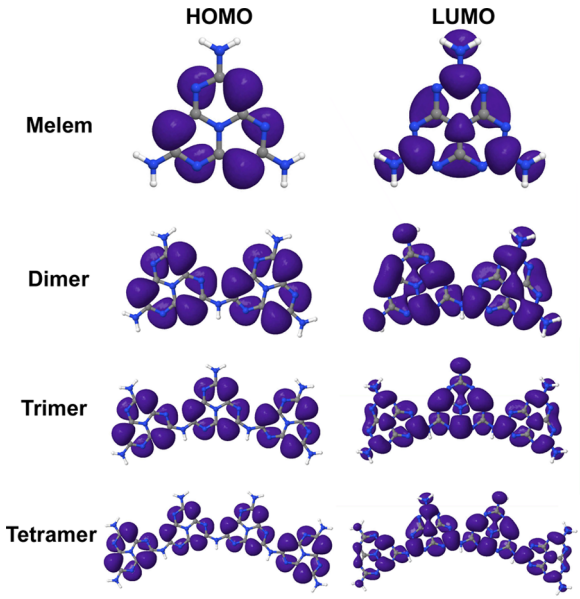

Figure 6. Highest occupied and lowest unoccupied orbitals of the monomer to the tetramer. Only the positive parts of the HOMO / LUMO orbitals are shown.

7.93 (2.77) eV for the trimer and 8.15 (2.95) eV and 8.98 (3.50) eV for the di- and monomer, respectively. From the PL spectra, both the oligomeric fractions and the polymer possess an emission state at about 375 nm but differ for the emission in the visible region. The polymer has an emission at 455 nm, while the spectra for the oligomers have a shoulder in the main emission peak at around 425 nm. The energy gap for these emissions corresponds to 2.7 eV for the polymer and 2.9 eV for the oligomers. While the absolute agreement with DFT-PBE is fortuitous, again the trend with length is in good agreement with the computational results. This shift in energy level is due to the LUMO shifting to more positive energy while the HOMO shifts much less with oligomer length, implying that the photoelectrons in the shorter oligomer are thermodynamically more reducing than the longer ones (i.e., more driving force for electron transfer), while the photoholes have largely invariant oxidizing ability. In relating this LUMO shift to the activity, we find that the absorption edge from the UV−vis spectra for the oligomeric fractions (440 nm, 2.8 eV) is blue-shifted by about 20 nm (0.1 eV) from the polymer (460 nm, 2.7 eV). Likewise for the PL, the emission is blue-shifted by 30 nm (0.2 eV) going from the polymer to the oligomer. In other words, the oligomer fraction has an over 5-fold increase in hydrogen evolution rate over melon (Figure 5; 2-fold on a per surface area basis) with only about 100−200 mV potential change. This variation is large, considering that semiconductor photocatalysts exhibit far less than a 2-fold variation in activity for a similar shift in band potential resulting from quantum confinement or by varying the composition of solid solution.[66−69] Thus, in addition to the slightly higher reducing ability of the photoelectron due to the LUMO shift, we also considered factors related to kinetics, such as the location and distribution of the charge transfer sites. We find that for all oligomers the location of the HOMO, which is likely associated with the oxidation sites where the photoholes are quenched after interaction with methanol as the sacrificial electron donor, is localized exclusively on the tertiary heptazine nitrogen atoms for the small oligomers (Figure 6 and Table S4, Supporting Information).[6,58] Since these are the positions where direct hydrogen bonding interactions to methanol are most likely to occur, the HOMO location is therefore "ideal" for all oligomers. However, for all oligomers calculated, the LUMO, which typically is used as an approximation for the reducing sites,[70] is delocalized across the carbon and nitrogen atoms of the heptazine, including the central nitrogen and the bridging secondary amine, as well as localized on the primary amines. The LUMO is not equally spread across the multiple heptazine units of the oligomer, i.e., not entirely delocalized; even stronger localization effects are observed when conformational variations[71] are accounted for (see Table S4, Supporting Information), consistent with the "quasi-monomer" description.[47] An explanation consistent with our empirical results would be to consider the primary and/or secondary amines to be the primary reducing sites, as they are not only more prevalent in the oligomeric than the polymeric case but better exposed on account of the stacking disorder and conformational flexibility for the less condensed oligomer, as observed in the broad XRD reflections. These amine groups would also be the preferred site for the in situ reduction of Pt^0 from $PtCl_6^{2-}$, given the numerous literature precedents on the encapsulation of platinum particles within photo- and electrocatalytic amine-bearing matrices (e.g., dendrimer[72−75] and metal organic framework[76]). These amines allow either better coordination to the platinum centers for efficient electron transfer (e.g., via inner sphere electron transfer mechanism), or for amine-mediated proton-coupled electron transfer,[77] or even as the actual site for recombination of the hydrogen atoms to molecular hydrogen.[78]

These findings therefore lend evidence to the often-invoked relevance of "defects", which are commonly considered to increase the photocatalytic activity of carbon nitrides, as the nature of such defects can in fact be associated with polymer terminations and increased exposure of the peripheral functional groups (e.g., $-NH_2$). It will therefore be key to explore whether the most NH_2-rich species—melem and its derivatives—possess photocatalytic activity, and how the modification of the heptazine skeleton affects the optoelectronic and photocatalytic properties. From a computational approach, it will be instructive to investigate conformer dependency, as observed in the preliminary calculations for the tetramer (Table S4, Supporting Information), where symmetry breaking and hydrogen bonding have been shown to shift both the HOMO/LUMO energy and location, and thus may offer alternative strategies for activity increase through altered photogenerated charge carrier location and separation.

The high activity of our experimentally resolved oligomer fractions highlights the potential of active site engineering as an alternative strategy to improve the intrinsic photocatalytic activity of carbon nitrides. The hydrogen evolution rates of these oligomers are quite competitive with values in the literature (after normalizing for catalyst loading and surface area), which are typically in the range of 1−4 μmol H_2 h^{-1} m^{-2} for g-C_3N_4 that is composited with other semiconductors.[27,30,31,50] Note that a direct comparison is difficult on account of differences in reaction parameters (electron donor used, reactor configuration, and whether the catalyst loading is limited by mass transfer[79]). Nonetheless, we expect the activity of the oligomer can be further enhanced on a per weight basis provided that the active phase can be selectively synthesized. We note that these two "oligomeric" fractions constitute approximately 50 wt % of the as-synthesized sample, with about

DOI: 10.1021/ja511802c
J. Am. Chem. Soc. 2015, 137, 1064−1072

half of the melem remaining unreacted even after 12 h at 450 °C. We foresee that the yield and polymerization degree are far from optimized, and a simple fine-tuning of the synthesis parameters may already provide ample scope for further improvement in the photocatalytic activity of these heptazine-based polymers.

CONCLUSIONS

We have experimentally demonstrated that the length of the melon polymer chain can be reduced by decreasing the synthesis temperature, yielding a hydrogen evolution photocatalyst with 3 times the activity of the polymer under AM 1.5 conditions, despite absorbing less in the visible region. Through a separation procedure and detailed characterization, this photocatalyst was shown to be a mixture of the monomer and oligomers of melem. The former has negligible activity, while the latter has nearly twice the activity of the as-synthesized material on a per weight basis, resulting in a total increase in activity of 6 times the polymer. Moreover, the photocatalytic activity appears to increase with shorter oligomer length to a certain point, consistent with the periphery of the heptazine moiety being involved in the catalytic reaction, which has been corroborated by DFT calculations. The successful isolation of the active component(s) demonstrated in this work provides a platform for future investigations into the catalytic properties of carbon nitride photocatalysts. Furthermore, these results illustrate a strategy based on active site engineering for intrinsically improving carbon nitride photocatalysts, thus highlighting the need for developing synthetic protocols selective to the active species.

EXPERIMENTAL SECTION

Detailed descriptions of the characterization techniques are provided in the Supporting Information.

A sample tentatively notated as "melem oligomer" was prepared as follows. Melamine (1.00 g, Carl Roth, >99%) was loaded into a loosely covered alumina boat and was placed into a quartz tube furnace. After complete removal of air by an extended argon purge, the furnace was heated under a slow argon flow to 450 °C for 12 h at a 5 °C min^{-1} ramp and then allowed to cool to ambient temperature at an unrestricted rate. The resulting light yellow solid (390 mg) was then thoroughly ground with an agate mortar and pestle prior to characterization and photocatalytic evaluation. The crystallinity of the product can be improved by further heat treatment at 300 °C for 24 h in argon.

For comparison, a sample of melon was prepared in an identical fashion, except that melamine was heated to 550 °C.

Separation of the melem oligomer into different fractions was carried out by stirring 400 mg of the ground solid in DMSO (100 mL) for 1 week. The resulting suspension was centrifuged at a relative centrifugal force (RCF) of 10000. The precipitate (notated as "fraction RCF 10000") was washed with acetone and dried at 100 °C. The supernatant was centrifuged again at a RCF of 60000, and the precipitate (fraction RCF 60000) was washed and dried as in the previous fraction. For the supernatant, the DMSO was completely evaporated off at 70 °C *in vacuo* and the resulting white powder was subjected to the same acetone wash and drying procedure as described above for the two other fractions.

ASSOCIATED CONTENT

Supporting Information

Details of the Experimental Section and theoretical calculations, and additional characterizations (XPS, elemental analyses, surface areas, TGA-MS, SEM, and PL) of the melem oligomer and of the isolated species from differential centrifugation. This material is available free of charge via the Internet at http://pubs.acs.org.

AUTHOR INFORMATION

Corresponding Author

*b.lotsch@fkf.mpg.de

Notes

The authors declare no competing financial interest.

ACKNOWLEDGMENTS

V.W.-h.L. gratefully acknowledges a postdoctoral scholarship from the Max Planck Society. This work was supported by the Deutsche Forschungsgemeinschaft (projects LO1801/1-1, SE1417/5-1), the Max Planck Society, the cluster of excellence Nanosystems Initiative Munich (NIM), the Fonds der Chemischen Industrie (FCI), and the Center for Nanoscience (CeNS). The authors would like to thank Dr. Stephan Rauschenbach for assistance in the preparation and analysis of the samples for MALDI-TOF measurements. The authors would also like to thank Ms. Marie-Luise Schreiber for the elemental analyses, Dr. Konuma for the XPS analyses, and Mr. Daniel Weber for the TGA-MS experiments. This work is dedicated to Prof. Arndt Simon on the occasion of his 75th birthday.

REFERENCES

(1) Rand, D. A. J.; Dell, R. M. *Hydrogen Energy: Challenges and Prospects*; RSC Publishing: Cambridge, U.K., 2008.
(2) Fujishima, A.; Honda, K. *Nature* **1972**, *238*, 37.
(3) Kato, H.; Asakura, K.; Kudo, A. *J. Am. Chem. Soc.* **2003**, *125*, 3082.
(4) Lu, D.; Takata, T.; Saito, N.; Inoue, Y.; Domen, K. *Nature* **2006**, *440*, 295.
(5) Maeda, K.; Domen, K. *J. Phys. Chem. C* **2007**, *111*, 7851.
(6) Wang, X.; Maeda, K.; Thomas, A.; Takanabe, K.; Xin, G.; Carlsson, J. M.; Domen, K.; Antonietti, M. *Nat. Mater.* **2009**, *8*, 76.
(7) Wang, Y.; Wang, X.; Antonietti, M. *Angew. Chem., Int. Ed.* **2012**, *51*, 68.
(8) Cao, S.; Yu, J. *J. Phys. Chem. Lett.* **2014**, *5*, 2101.
(9) Liu, A. Y.; Cohen, M. L. *Science* **1989**, *245*, 841.
(10) Jürgens, B.; Irran, E.; Senker, J.; Kroll, P.; Müller, H.; Schnick, W. *J. Am. Chem. Soc.* **2003**, *125*, 10288.
(11) Lotsch, B. V.; Schnick, W. *Chem. Mater.* **2005**, *17*, 3976.
(12) Lotsch, B. V.; Schnick, W. *Chem. Mater.* **2006**, *18*, 1891.
(13) Sattler, A.; Schnick, W. *Z. Anorg. Allg. Chem.* **2006**, *632*, 238.
(14) Lotsch, B. V.; Döblinger, M.; Sehnert, J.; Seyfarth, L.; Senker, J.; Oeckler, O.; Schnick, W. *Chem.—Eur. J.* **2007**, *13*, 4969.
(15) Lotsch, B. V.; Schnick, W. *Chem.—Eur. J.* **2007**, *13*, 4956.
(16) Seyfarth, L.; Seyfarth, J.; Lotsch, B. V.; Schnick, W.; Senker, J. *Phys. Chem. Chem. Phys.* **2010**, *12*, 2227.
(17) Chen, X.; Jun, Y.-S.; Takanabe, K.; Maeda, K.; Domen, K.; Fu, X.; Antonietti, M.; Wang, X. *Chem. Mater.* **2009**, *21*, 4093.
(18) Wang, X.; Maeda, K.; Chen, X.; Takanabe, K.; Domen, K.; Hou, Y.; Fu, X.; Antonietti, M. *J. Am. Chem. Soc.* **2009**, *131*, 1680.
(19) Li, X.-H.; Zhang, J.; Chen, X.; Fischer, A.; Thomas, A.; Antonietti, M.; Wang, X. *Chem. Mater.* **2011**, *23*, 4344.
(20) Niu, P.; Zhang, L.; Liu, G.; Cheng, H.-M. *Adv. Funct. Mater.* **2012**, *22*, 2763.
(21) Wu, G.; Thind, S. S.; Wen, J.; Yan, K.; Chen, A. *Appl. Catal., B* **2013**, *142−143*, 590.
(22) Yang, S.; Gong, Y.; Zhang, J.; Zhan, L.; Ma, L.; Fang, Z.; Vajtai, R.; Wang, X.; Ajayan, P. M. *Adv. Mater.* **2013**, *25*, 2452.
(23) Liu, G.; Niu, P.; Sun, C.; Smith, S. C.; Chen, Z.; Lu, G. Q. M.; Cheng, H.-M. *J. Am. Chem. Soc.* **2010**, *132*, 11642.
(24) Zhang, J.; Sun, J.; Maeda, K.; Domen, K.; Liu, P.; Antonietti, M.; Fu, X.; Wang, X. *Energy Environ. Sci.* **2011**, *4*, 675.

DOI: 10.1021/ja511802c
J. Am. Chem. Soc. 2015, 137, 1064−1072

(25) Zhang, G.; Zhang, J.; Zhang, M.; Wang, X. *J. Mater. Chem.* **2012**, *22*, 8083.
(26) Zhang, J.; Zhang, G.; Chen, X.; Lin, S.; Möhlmann, L.; Dołęga, G.; Lipner, G.; Antonietti, M.; Blechert, S.; Wang, X. *Angew. Chem., Int. Ed.* **2012**, *51*, 3183.
(27) Di, Y.; Wang, X.; Thomas, A.; Antonietti, M. *ChemCatChem* **2010**, *2*, 834.
(28) Ding, Z.; Chen, X.; Antonietti, M.; Wang, X. *ChemSusChem* **2011**, *4*, 274.
(29) Xiang, Q.; Yu, J.; Jaroniec, M. *J. Phys. Chem. C* **2011**, *115*, 7355.
(30) Ge, L.; Zuo, F.; Liu, J.; Ma, Q.; Wang, C.; Sun, D.; Bartels, L.; Feng, P. *J. Phys. Chem. C* **2012**, *116*, 13708.
(31) Kang, H. W.; Lim, S. N.; Song, D.; Park, S. B. *Int. J. Hydrogen Energy* **2012**, *37*, 11602.
(32) Sun, L.; Zhao, X.; Jia, C.-J.; Zhou, Y.; Cheng, X.; Li, P.; Liu, L.; Fan, W. *J. Mater. Chem.* **2012**, *22*, 23428.
(33) Cao, S.-W.; Yuan, Y.-P.; Barber, J.; Loo, S. C. J.; Xue, C. *Appl. Surf. Sci.* **2014**, *319*, 344.
(34) Chen, J.; Shen, S.; Guo, P.; Wang, M.; Wu, P.; Wang, X.; Guo, L. *Appl. Catal., B* **2014**, *152*−*153*, 335.
(35) Döblinger, M.; Lotsch, B. V.; Wack, J.; Thun, J.; Senker, J.; Schnick, W. *Chem. Commun.* **2009**, 1541.
(36) Sattler, A.; Pagano, S.; Zeuner, M.; Zurawski, A.; Gunzelmann, D.; Senker, J.; Müller-Buschbaum, K.; Schnick, W. *Chem.—Eur. J.* **2009**, *15*, 13161.
(37) Wirnhier, E.; Döblinger, M.; Gunzelmann, D.; Senker, J.; Lotsch, B. V.; Schnick, W. *Chem.—Eur. J.* **2011**, *17*, 3213.
(38) Makowski, S. J.; Köstler, P.; Schnick, W. *Chem.—Eur. J.* **2012**, *18*, 3248.
(39) Ham, Y.; Maeda, K.; Cha, D.; Takanabe, K.; Domen, K. *Chem.—Asian J.* **2013**, *8*, 218.
(40) Schwinghammer, K.; Tuffy, B.; Mesch, M. B.; Wirnhier, E.; Martineau, C.; Taulelle, F.; Schnick, W.; Senker, J.; Lotsch, B. V. *Angew. Chem., Int. Ed.* **2013**, *52*, 2435.
(41) Schwarzer, A.; Saplinova, T.; Kroke, E. *Coord. Chem. Rev.* **2013**, *257*, 2032.
(42) Bojdys, M. J. Ph.D. Thesis, Max-Planck Institut für Kolloid- und Grenzflächenforschung, Potsdam, Germany, 2009.
(43) Maeda, K.; Wang, X.; Nishihara, Y.; Lu, D.; Antonietti, M.; Domen, K. *J. Phys. Chem. C* **2009**, *113*, 4940.
(44) Sabio, E. M.; Chamousis, R. L.; Browning, N. D.; Osterloh, F. E. *J. Phys. Chem. C* **2012**, *116*, 3161.
(45) Osterloh, F. E. *Chem. Soc. Rev.* **2013**, *42*, 2294.
(46) Yang, F.; Kuznietsov, V.; Lublow, M.; Merschjann, C.; Steigert, A.; Klaer, J.; Thomas, A.; Schedel-Niedrig, T. *J. Mater. Chem. A* **2013**, *1*, 6407.
(47) Merschjann, C.; Tyborski, T.; Orthmann, S.; Yang, F.; Schwarzburg, K.; Lublow, M.; Lux-Steiner, M.-C.; Schedel-Niedrig, T. *Phys. Rev. B* **2013**, *87*, 205204.
(48) Schwarzer, A.; Böhme, U.; Kroke, E. *Chem.—Eur. J.* **2012**, *18*, 12052.
(49) Guo, Y.; Chu, S.; Yan, S.; Wang, Y.; Zou, Z. *Chem. Commun.* **2010**, *46*, 7325.
(50) Yuan, Y.-P.; Xu, W.-T.; Yin, L.-S.; Cao, S.-W.; Liao, Y.-S.; Tng, Y.-Q.; Xue, C. *Int. J. Hydrogen Energy* **2013**, *38*, 13159.
(51) Komatsu, T. *J. Mater. Chem.* **2001**, *11*, 799.
(52) Tyborski, T.; Merschjann, C.; Orthmann, S.; Yang, F.; Lux-Steiner, M.-C.; Schedel-Niedrig, T. *J. Phys.: Condens. Matter* **2012**, *24*, 162201.
(53) Thomas, A.; Fischer, A.; Goettmann, F.; Antonietti, M.; Müller, J.-O.; Schlögl, R.; Carlsson, J. M. *J. Mater. Chem.* **2008**, *18*, 4893.
(54) Ishii, A.; Habu, K.; Kishi, S.; Ohtsu, H.; Komatsu, T.; Osaka, K.; Kato, K.; Kimura, S.; Takata, M.; Hasegawa, M.; Shigesato, Y. *Photochem. Photobiol. Sci.* **2007**, *6*, 804.
(55) Lotsch, B. V. Ph.D. Thesis, Ludwig Maximilians Universität, München, Germany, 2006.
(56) Komatsu, T. *Macromol. Chem. Phys.* **2001**, *202*, 19.
(57) Xing, J.; Fang, W. Q.; Zhao, H. J.; Yang, H. G. *Chem.—Asian J.* **2012**, *7*, 642.
(58) Huda, M. N.; Turner, J. A. *J. Appl. Phys.* **2010**, *107*, 123703.
(59) Meek, G. A.; Baczewski, A. D.; Little, D. J.; Levine, B. G. *J. Phys. Chem. C* **2014**, *118*, 4023.
(60) Reshak, A. H.; Khan, S. A.; Auluck, S. *RSC Adv.* **2014**, *4*, 6957.
(61) Perdew, J. P.; Burke, K.; Ernzerhof, M. *Phys. Rev. Lett.* **1996**, *77*, 3865.
(62) Tkatchenko, A.; Scheffler, M. *Phys. Rev. Lett.* **2009**, *102*, 073005.
(63) Atalla, V.; Yoon, M.; Caruso, F.; Rinke, P.; Scheffler, M. *Phys. Rev. B* **2013**, *88*, 165122.
(64) Blum, V.; Gehrke, R.; Hanke, F.; Havu, P.; Havu, V.; Ren, X.; Reuter, K.; Scheffler, M. *Comput. Phys. Commun.* **2009**, *180*, 2175.
(65) Ren, X.; Rinke, P.; Blum, V.; Wieferink, J.; Tkatchenko, A.; Sanfilippo, A.; Reuter, K.; Scheffler, M. *New J. Phys.* **2012**, *14*, 053020.
(66) Lee, H.-S.; Woo, C.-S.; Youn, B.-K.; Kim, S.-Y.; Oh, S.-T.; Sung, Y.-E.; Lee, H.-I. *Top. Catal.* **2005**, *35*, 255.
(67) Datta, A.; Priyam, A.; Bhattacharyya, S. N.; Mukherjea, K. K.; Saha, A. *J. Colloid Interface Sci.* **2008**, *322*, 128.
(68) Luo, W.; Li, Z.; Jiang, X.; Yu, T.; Liu, L.; Chen, X.; Ye, J.; Zou, Z. *Phys. Chem. Chem. Phys.* **2008**, *10*, 6717.
(69) Zhang, G.; Monllor-Satoca, D.; Choi, W. *Catal. Sci. Technol.* **2013**, *3*, 1790.
(70) Ceroni, P.; Balzani, V. In *The Exploration of Supramolecular Systems and Nanostructures by Photochemical Techniques*; Ceroni, P., Ed.; Springer: Dordrecht, The Netherlands, 2012.
(71) Butchosa, C.; Guiglion, P.; Zwijnenburg, M. A. *J. Phys. Chem. C* **2014**, *118*, 24833.
(72) Ye, H.; Scott, R. W. J.; Crooks, R. M. *Langmuir* **2004**, *20*, 2915.
(73) Esumi, K.; Suzuki, A.; Yamahira, A.; Torigoe, K. *Langmuir* **2000**, *16*, 2604.
(74) Yang, L.; Luo, Y.; Jia, X.; Ji, Y.; You, L.; Zhou, Q.; Wei, Y. *J. Phys. Chem. B* **2004**, *108*, 1176.
(75) Zhao, M.; Crooks, R. M. *Adv. Mater.* **1999**, *11*, 217.
(76) Wen, M.; Mori, K.; Kamegawa, T.; Yamashita, H. *Chem. Commun.* **2014**, *50*, 11645.
(77) DuBois, M. R.; DuBois, D. L. *Chem. Soc. Rev.* **2009**, *38*, 62.
(78) Joo, J. B.; Dillon, R.; Lee, I.; Yin, Y.; Bardeen, C. J.; Zaera, F. *Proc. Natl. Acad. Sci. U.S.A.* **2014**, *111*, 7942.
(79) Maschmeyer, T.; Che, M. *Angew. Chem., Int. Ed.* **2010**, *49*, 1536.

DOI: 10.1021/ja511802c
J. Am. Chem. Soc. 2015, 137, 1064−1072